U–Pb Dating of Zircon and Zirconolite Inclusions in Marble-Hosted Gem-Quality Ruby and Spinel from Mogok, Myanmar

Myint Myat Phyo [1,2], Hao A.O. Wang [2,*], Marcel Guillong [3], Alfons Berger [4], Leander Franz [1,*], Walter A. Balmer [2] and Michael S. Krzemnicki [2]

1. Department of Environmental Sciences, Mineralogy and Petrology, University of Basel, Bernoullistrasse 30, 4056 Basel, Switzerland; myint.myatphyo@ssef.ch
2. Swiss Gemmological Institute SSEF, Aeschengraben 26, 4051 Basel, Switzerland; info@collectionbalmer.com (W.A.B.); director@ssef.ch (M.S.K.)
3. Institute of Geochemistry and Petrology, ETH Zurich, Clausiusstrasse 25, 8092 Zürich, Switzerland; marcel.guillong@erdw.ethz.ch
4. Institute of Geological Sciences, University of Bern, Baltzerstrasse 1+3, 3012 Bern, Switzerland; alfons.berger@geo.unibe.ch
* Correspondence: hao.wang@ssef.ch (H.A.O.W.); leander.franz@unibas.ch (L.F.); Tel.: +41-61-262-06-40 (H.A.O.W.)

check for updates

Abstract: The Mogok area in Myanmar (Burma) is known since historic times as a source for some of the finest rubies and spinels in the world. In this study, we focus on in-situ U–Pb geochronological analyses of zircon and zirconolite, either present as inclusions in gem-quality ruby and spinel or as accessory minerals in ruby- and spinel-bearing marble and adjacent granulite facies gneisses. The age determination was carried out using both laser ablation inductively coupled plasma time-of-flight mass spectrometry (LA-ICP-TOF-MS) and sector-field mass spectrometry (LA-ICP-SF-MS). In addition, we present multi-element data (REE) of zircon and zirconolite collected with LA-ICP-TOF-MS to further characterize these inclusions. Most of the studied zircon grains display growth zoning (core/rim) regardless if as inclusion in gemstones, or as accessory mineral in host rock samples. U–Pb dating was conducted on both core and rim of zircon grains and revealed most ages ranging from ~200 Ma in the core to ~17 Ma in the rim. The youngest U–Pb ages determined from the rim of zircon inclusions in gem-quality ruby and spinel are 22.26 ± 0.36 Ma and 22.88 ± 0.72 Ma, respectively. This agreement in U–Pb ages is interpreted to indicate a simultaneous formation of ruby and spinel in the Mogok area. In ruby- and spinel-bearing marble from Bawlongyi, the youngest zircon age was determined as 17.11 ± 0.22 Ma. Furthermore, U–Pb age measured on the rim of zircon grains in a biotite-garnet gneiss reveals a Late Oligocene age (26.13 ± 1.24 Ma), however older ages up to Precambrian age were also recorded in the cores of zircon as accessory minerals from this gneiss. These old ages point to a detrital origin of the analysed zircon cores. Although non-matrix matched standard was applied, zirconolite U–Pb age results are narrower in distribution from ~35 Ma to ~17 Ma, falling within the range of zircon ages. Based on results which are well in accordance with previous geochronological data from the Mogok Metamorphic Belt (MMB), we deduce that gem-quality ruby and spinel from Mogok probably formed during a granulite-facies regional metamorphic event in Oligocene to Early Miocene, related to post collision tectonics of the Eurasian and Indian plates. Our data not only provide key information to understand the formation of gem-quality ruby and spinel in the so-called Mogok Stone Tract, but also provide assisting evidence when determining the country of origin of gemstones in gemmological laboratories.

Keywords: ruby; spinel; Mogok; geochronology; U–Pb dating; zircon; zirconolite

1. Introduction

Ruby, the chromium-bearing red variety of corundum (Al_2O_3) and chromium-bearing red spinel ($MgAl_2O_4$) are among the world's most valued gemstones. In the gem trade, the price of a ruby and spinel is not only defined by their size and quality, but also to a large part by their geographic (country of) origin, notably when they are from a historically important and famed gem deposit. Ruby and spinel of gem-quality from marble-hosted deposits are known from a number of localities, such as the Mogok area (Figure 1) and Mong Hsu in Myanmar, the Hunza Valley in Pakistan, Jegdalek in Afghanistan, Murgab in Tajikistan, Luc Yen in Vietnam and the Morogoro region in Tanzania. From these deposits, the Mogok area is considered by far the most important and historically reputed source for ruby and spinel in the trade. This explains, why in literature corundum (ruby and sapphire) and to a lesser extent spinel from Mogok have been extensively studied, either gemmologically and in general [1–4], or focusing specifically on trace elements [5,6], stable isotopes [7–10], solid inclusions [11] and fluid inclusions [12]. In geochronology, a number of studies were published about the Mogok area or further gem deposits worldwide, either investigating minerals related to gemstone formation or inclusions in rough and faceted gemstones [13–21].

Figure 1. Faceted gem-quality ruby (0.369 ct) and rough ruby crystal within marble from Mogok area, Myanmar. Photo: M.M.P.

In recent years, U–Pb dating of inclusions (e.g., zircon, titanite, etc.) in gemstones using laser ablation inductively coupled plasma mass spectrometry (LA-ICP-MS) has become more popular due to easier access to instrumentation, minimum sample preparation, smaller laser crater size and improved instrument sensitivity [22,23]. The U–Pb ages of inclusions found in a gemstone indicate the maximum possible formation age of that gemstone. As such, these radiometric ages may provide gemmological laboratories with additional evidence when carrying out country of origin determination as a commercial service to the gem trade. This is especially helpful when separating ruby, sapphire and spinel related to the Himalayan orogenesis (e.g., Mogok area in Myanmar) from those related to the much older Pan-African orogeny (e.g., Morogoro area in Tanzania) [17,19,24–26].

For the Mogok area, only a limited amount of geochronological data from inclusions in gemstones and from accessory minerals in host rocks have been published so far: zircon inclusion in ruby ~32 Ma [16], titanite in ruby ~32 Ma [14], zircon in sapphire ~27 Ma [24], zircon in granitic host rocks ~16.8 Ma [26]. More geochronological data from this gem-rich area is thus still essential in order to

get a better understanding of its complex geology and to be able to compile a genetic model for the formation of gemstones in the Mogok area.

In this paper, we present new U–Pb ages of zircon and zirconolite, found as inclusions in gem-quality ruby and spinel or as accessory minerals in host rock samples from the Mogok area. In addition, we present rare earth element data (REE) of selected zircon and zirconolite grains for further characterization. Our data contributes to a better understanding of the complex geological processes resulting in the formation of gem-quality ruby and spinel in the studied area. Furthermore, our data may assist gemmological laboratories specifically in country of origin determination.

2. Regional Geological Setting

The Mogok Metamorphic Belt (MMB), further described in early studies [27,28], is a large sickle-shaped belt of regionally metamorphosed rocks stretching N-S from central to upper Myanmar as the southern continuation of the Himalayan syntaxis [29]. It forms the western margin of the Shan-Thai Block (Sibumasu Block) and is adjacent to the north-south trending right-lateral strike-slip Sagaing Fault, related to the youngest Cenozoic metamorphic events [30]. The Mogok-Mandalay-Mergui Belt extends to the Mergui area in the southern part of Myanmar [31,32]. In the so-called Mogok Stone Tract [27], located at the northeastern end of the MMB, there is an accumulation of world-renowned gem deposits, namely of rubies, sapphires and spinels [3,28]. The formation of those gemstones is related to late-stage Cenozoic metamorphic events within this geological unit [30,33,34]. The Mogok area mainly consists of upper amphibolite to granulite facies marbles, schists and gneisses [35]. Amongst these, the Mogok gneisses [27] in the southern part of the Mogok area are considered to be the oldest rock units in this area of Myanmar [36]. Gem-quality ruby and spinel are found in the Mogok area in both primary deposits in marbles and secondary deposits in alluvial and eluvial placers, as well as accumulated placers in karstic sinkholes and caverns [37].

The MMB has been extensively studied with a main focus on regional geology, geochemistry and geochronology [30,33,38–40]. In terms of geochronology, the ruby- and spinel-bearing marbles from the Mogok area are stratigraphically interpreted in previous studies [27,28] as being metamorphosed limestones of Precambrian age. Searle and Haq considered the Mogok metasediments to be originally Precambrian to Jurassic rocks of the Shan Plateau [41], whereas Clegg described them as mid-Cretaceous limestones and Jurassic sediments [42]. From the Precambrian to Cenozoic, the MMB experienced several magmatic and metamorphic events, which are commonly summarized as: Precambrian to Palaeozoic regional metamorphism and magmatism indicated by Ordovician age on zircon from foliated leucogranite [2] and Late Cambrian age on biotite gneiss [21] as well as Jurassic magmatism on biotite augen gneiss [40]. The latest, high-grade regional metamorphic event in the MMB occurred in Paleogene to Early Neogene due to the collision of the Sibumasu Block with the West Burma Block subsequent to the collision of the Indian and the Asian plates [43,44] and was followed by an intense episode of post-tectonic magmatism [2,26,45].

3. Materials and Methods

3.1. Zircon and Zirconolite
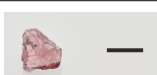
Prior to analyses, all gemstone samples (ruby and spinel) were polished to expose zircon and zirconolite inclusions. For host rocks, samples were first embedded in epoxy, before being polished.

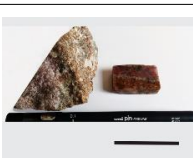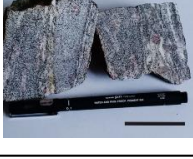The zircon and zirconolite inclusions were identified using a standard gemmological microscope (StereoZoom7, Cambridge Instruments, Cambridge, UK) and a polarization microscope (Leica DMLS, Wetzlar, Germany), two Raman micro-spectrometers (Renishaw inVia equipped with an argon-ion laser at 514.5 nm; Swiss Gemmological Institute SSEF, Basel, Switzerland; Bruker Senterra with a Nd-YAG laser at 532 nm; Department of Environmental Sciences, Mineralogy and Petrology, University of Basel, Basel, Switzerland), and a scanning electron microscope (FEI Nova Nano SEM 230, Nano Imaging Lab, University of Basel, Basel, Switzerland) equipped with an energy-dispersive spectrometer (EDS)

and a back-scattered electron detector (BSE). In order to avoid any contamination, the samples were not coated. More details about the analytical conditions applied for Raman and SEM analyses are described in our previous publication on spinel inclusions from Mogok [11].

Zircon ($ZrSiO_4$) is found as inclusion in gem-quality ruby and spinel and as accessory mineral in three host rock samples (ruby- and spinel-bearing marble from Bawlongyi area, granulite-facies gneiss from Aunglan Taung area in central Mogok and granulite-facies gneiss from Kinn area in western Mogok, see Table 1).

Table 1. List of samples from Mogok investigated for this study. The scale bars represent 5 mm length for gemstones and 5 cm for host rocks.

Sample Name	Locality	Host Material	Analysed Grain	Weight (ct)	Sample Photo
SSEF96663_A	Mansin		4 Zircons and 5 Zirconolites	2.411	
SSEF96666_A	Kadotetat		1 Zircon	2.431	
SSEF96666_B		Ruby	1 Zircon	1.270	
SSEF96667_A	Kyatpyin		1 Zircon	1.615	
SSEF96668_A	Kyaukpoke		1 Zircon	0.268	
SSEF92720_D	Kyauksaung		2 Zircons	0.405	
SSEF92725_D	Kyauksin	Spinel	2 Zircons	0.673	
SSEF92725_E			1 Zircon	0.940	
BLG_12	Bawlongyi	Ruby- and Spinel-bearing Marble	32 Zircons and 9 Zirconolites		
ALT_03	Aunglan Taung	Gneiss	40 Zircons		
K_01	Kinn		24 Zircons		

Only 5 from a total of 85 ruby samples as well as 3 from 100 spinels contained zircon inclusions suitable for dating in terms of size and proximity to the sample's surface. Most of the observed zircon inclusions in the examined gemstone samples however were either too small (<10 μm) or located too deep inside the sample to be reached by laser ablation and therefore could not be considered for U–Pb dating in this study. In total, 8 zircon inclusions from ruby and 5 zircon inclusions from spinel were analysed for this study. The size of the analysed zircon grains in ruby range from 50 to 300 μm in diameter. In contrast to this, the zircon grains in spinel are smaller with a maximum diameter of 50 μm, with some inclusions being as small as 10 μm. In addition to the zircon inclusions from gemstones, we have studied zircon present as accessory mineral in host-rocks. In the ruby- and spinel-bearing marble from Bawlongyi area (Figure 2), we analysed a total of 32 zircons, occurring either as individual grains or intergrown with zirconolite. Furthermore, we analysed 40 zircons found as accessory mineral in a garnet-orthopyroxene gneiss from Aunglan Taung and 24 zircon grains in biotite-garnet gneiss from the Kinn area (Figure 2). The size of the accessory zircons in the Aunglan Taung gneiss is 35 μm to 50 μm, while those from Kinn gneiss are even smaller with a size of 10 μm to maximum 35 μm [46].

Zirconolite, ideally $CaZrTi_2O_7$, is known in several polytypoids, such as zirconolite-3*O* (orthorhombic), zirconolite-3*T* (trigonal), zirconolite-2*M* (monoclinic) and non-crystalline (metamict) or undetermined polytypoid [47]. This latter option explains why we were not able to identify zirconolite in our study using Raman spectroscopy. In fact, they all revealed featureless (amorphous) Raman spectra. However, by analysing the major and minor elemental composition using SEM equipped with an EDS detector, we were able to positively identify the zirconolite grains present in our samples. We observed two types of zirconolite: (1) individual inclusion of 40 μm to 100 μm size in ruby from Mansin, and (2) intergrown with zircon in Bawlongyi marble (see Table 1). Here, zirconolite forms either a 10–50 μm thick rim around zircon or occurs as small (maximum 5 μm) amoeboid inclusions within zircon.
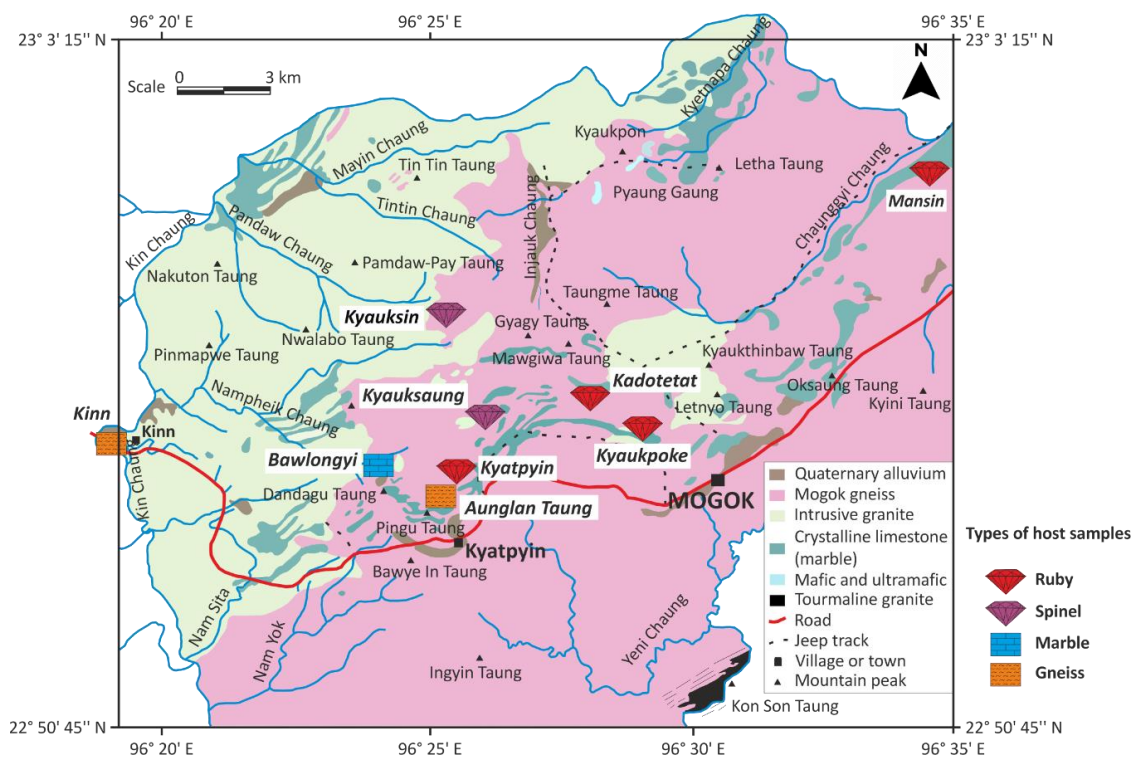

Figure 2. Sample locations plotted on the geological map of the Mogok area (modified after [28] and [48] with permission).

　　　To our knowledge, this study provides the first detailed characterization of zirconolite from the Mogok area. A detailed list of the zircon and zirconolite analysed and their occurrences are given in Table 1 and Supplementary Data.

3.2. Growth Zonation of Zircon and Zirconolite

　　　Zircon often shows complex growth zonation patterns. This may strongly influence radiometric dating if an analysis is conducted across growth zones of different ages [49]. In order to visualize such zoning in our zircon (and zirconolite) grains (Figure 3a,b) and to determine the appropriate position to carry out U–Pb dating, we additionally collected variable pressure secondary electron (VPSE) images using a ZEISS EVO 50 SEM (Institute of Geological Sciences, University of Bern, Bern, Switzerland). These images reveal three different types of patterns: (a) zircon with a characteristic core/rim growth zonation, (b) zircon showing an irregular zoning pattern and (c) zircon with no zonation detectable by VPSE imaging.
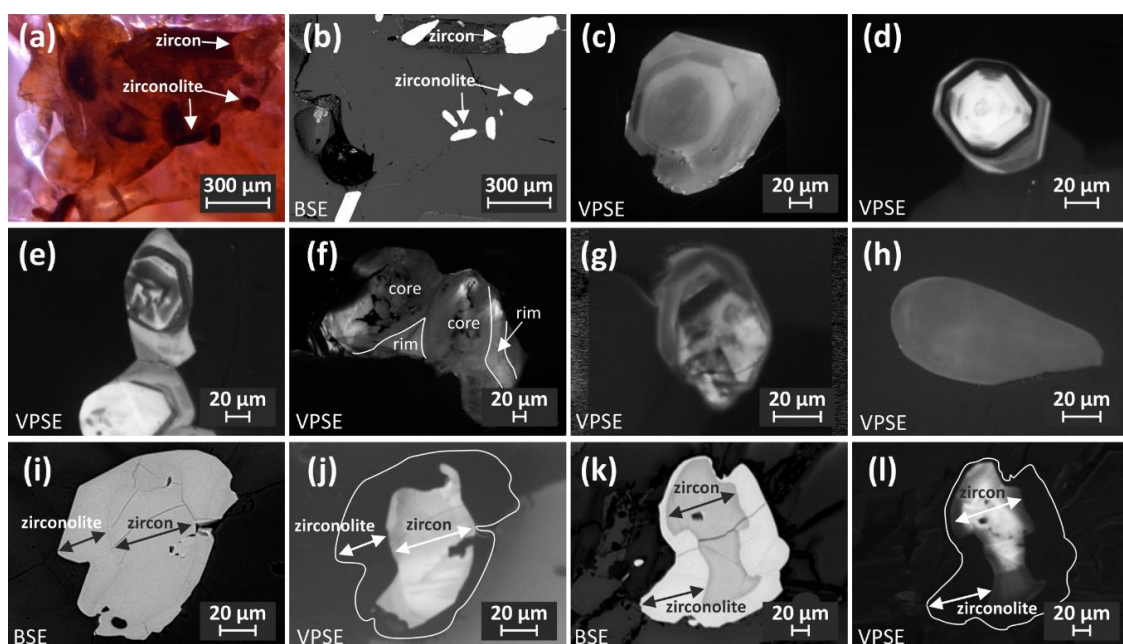
Figure 3. (**a**) Photomicrograph of zircon and zirconolite inclusion in ruby from Mansin, and (**b**) corresponding back-scattered electron (BSE) image. (**c**) Variable pressure secondary electron (VPSE) image of zircon inclusion in ruby from Kyatpyin with distinct core/rim zonation. (**d**,**e**) Similar core/rim zonation in VPSE images of accessory zircon from Aunglan Taung gneiss. (**f**) VPSE image of zircon inclusion in ruby from Mansin showing irregular zoning with an aggregated core and a homogeneous rim. (**g**) VPSE image of accessory zircon from Kinn gneiss showing irregular zoning. (**h**) VPSE image of zircon inclusion in spinel from Kyauksin revealing nearly no zoning. (**i**) BSE image of zircon and zirconolite intergrown in Bawlongyi marble (zirconolite occurs as a rim around zircon inclusion), and (**j**) their corresponding VPSE image. (**k**) BSE image of another zircon and zirconolite intergrowth in Bawlongyi marble and (**l**) their corresponding VPSE image.

　　　Distinct core/rim growth zonation is found in some zircon grains included in rubies from Kyatpyin (Figure 3c), but also in accessory zircons from gneisses (Figure 3d,e). The distinct core/rim growth zonation may indicate a magmatic origin of the core surrounded by a metamorphic rim. Such a zonation pattern is often observed, specifically in accessory zircon from gneiss [50]. Irregular zoning is found in zircon inclusions in ruby from the Mansin area (Figure 3f) revealing aggregated textures in the core and more homogeneous rim sections, but also in zircons present as accessory minerals in the studied gneisses (Figure 3g). BSE and VSPE images showing no (significant) growth zoning patterns are observed for zircon inclusions in spinel (Figure 3h), but also for the accessory zircons in

Bawlongyi marble (Figure 3i–l). This is also true for all investigated zirconolite grains. They show a homogeneous VPSE reaction and no zoning features, regardless if present as individual inclusion in ruby from Mansin or intergrown with zircon in Bawlongyi marble (Figure 3j,l).

3.3. LA-ICP-MS Instrumentations

For in-situ radiometric U–Pb dating and the multi-element characterization (specifically REE) of the zircon and zirconolite grains, a combined approach of two different mass spectrometer setups was applied to benefit from the advantages of each of these systems: (1) LA-ICP time-of-flight MS (LA-ICP-TOF-MS, Swiss Gemmological Institute SSEF, Basel, Switzerland) and (2) sector-field MS (LA-ICP-SF-MS, Institute of Geochemistry and Petrology, ETH Zurich, Zurich, Switzerland). Single detector SF-MS has about 15 times higher sensitivity compared to TOF-MS [51], hence a distinctly smaller laser spot can be used for analysis, minimizing potential overlaps of age zones, especially when analysing zoned zircon. Since the SF-MS data acquisition is sequential, only a limited number of masses can be collected. In contrast to this, TOF-MS allows simultaneous acquisition of the full mass spectrum, hence it is ideal for constant monitoring of elemental variations (e.g., when passing from one mineral to another), especially when the laser ablates into small mineral intergrowth. The drawback of this second method is its relatively lower sensitivity, thus requiring a larger laser ablation spot (e.g., 35 μm). Obviously, this last condition (laser spot size) of LA-ICP-TOF-MS is challenging, especially when analysing small zircon and zirconolite with narrow and/or complex growth zoning. Therefore, we applied LA-ICP-SF-MS for small and complex zoned zircon and for zirconolite, using a small spot size of only 13 to 19 μm and integration times of 10 ms (^{202}Hg, ^{208}Pb, ^{232}Th, ^{235}U, ^{238}U), 20 ms (^{204}Pb), 75 ms (^{207}Pb) and 90 ms (^{206}Pb), resulting in a total sweep time of 0.243 s (including MS settling time) for these eight selected isotopes of interest. In doing so, we were able to determine the different ages of the core and the rim of zoned zircon separately. The LA-ICP-TOF-MS system was then used for a detailed elemental and isotopic characterization of selected zircon and zirconolite grains, allowing the simultaneous acquisition of the full mass spectrum (^{7}Li$^+$ to ^{238}U$^+$) every 30 μs. For our analyses, 5000 full TOF-mass spectra were averaged and reported in one output data point (integration time 0.151 s). Data reduction of the TOF spectrum includes gas black correction, baseline correction based on two anchor points on both sides of the mass peak, as well as signal integration over a mass window (0.25 atomic mass unit), centred at the mass peak, in order to obtain the peak intensity (unit in mV) [52]. Further TOF- and SF-MS instrument parameters are listed in Supplementary Table S1.

For LA-ICP-SF-MS, we used the zircon standard GJ-1 (601.86 ± 0.37 Ma, from ^{206}Pb/^{238}U age results) [53,54] as a primary dating standard, with additional zircon secondary standards Plešovice (337.13 ± 0.37 Ma, ^{206}Pb/^{238}U age) [55], Temora 1 (416.8 ± 1.1 Ma, ^{206}Pb/^{238}U age) [56], Zircon 91500 (1063.51 ± 0.39 Ma, ^{206}Pb/^{238}U) [57]. The secondary reference zircon ages from measurements in this study are in accordance with published results. Data processing was carried out using software packages Iolite (version 2.5) [58] and VizualAge (version 2013-02) [59] for age calculation and uncertainty propagation. Laser induced element fractionation (LIEF) was corrected based on the primary reference material analysed with identical conditions as the sample. Unless otherwise mentioned, calculated ages are quoted as two times the standard error (2SE) and propagation of uncertainty is by quadratic addition. Reproducibility and age uncertainty of reference material are propagated where appropriate.

For TOF-MS, we employed an in-house zircon single crystal SSEF87244 with an age of 523 ± 5 Ma, as primary standard for U–Pb dating. This crystal was characterized by ICP-SF-MS to have a high uranium concentration (approximately U 2000 mg/kg) and having no detectable amount of common lead (^{204}Pb). The ages obtained from secondary standard Zircon 91500 (1059.62 ± 8.70 Ma, ^{206}Pb/^{238}U age) are in accordance with the published result within the uncertainty. For dating analyses of zirconolite, we applied the same set of zircon standards, due to the lack of a matrix-matched zirconolite standards. For data processing, we used an in-house developed calculation script based on MATLAB (R2018b, The MathWorks, Inc., Natick, MA, USA). Benefiting from the full mass spectrum analysis in TOF-MS, it was possible to recheck if the whole measurements were done on targeted inclusions

or if the ablation moved into host materials (ruby, spinel, etc.) by monitoring transient signals of various isotopes in TofDaq software (V1.2.97, TOFWERK AG, Thun, Switzerland). Furthermore, raw transient signals were carefully checked for common Pb interference based on isotope ^{204}Pb. In most of our samples, the ^{204}Pb signal was below the detection limit. Therefore, no correction for common Pb was applied. However, there may be still a small amount of common Pb present in our samples due to the low natural abundance of ^{204}Pb isotope, as shown in some discordant results in Wetherill and Tera-Wasserburg plots, and these discordant ages are omitted in the reported ages. The intensity ratios of U–Pb isotopes were monitored with TofDaq software to select appropriate sections in the transient signal that could be used for dating calculation. The radiometric ages based on ^{206}Pb/^{238}U and ^{207}Pb/^{235}U ratios are calculated using gas blank corrected signals. The radiometric ages are calculated as a ratio of the mean method and errors (2SE) are propagated following the procedures suggested by [60]. The age uncertainty of reference materials is propagated afterwards and other uncertainties are not included. All dating results are plotted using *IsoplotR* (V3.0) [61]. Analysis is accepted only when its age with 2SE overlaps the concordia curve [62]. For TOF-MS, the REEs were quantified using a non-matrix matched NIST610 SRM glass as external standard, due to its nearly full coverage of the periodic table of the elements. Additionally, Ca was used as internal standard and a total mass normalization procedure was applied [63].

4. Results

In total, we analysed 109 zircon grains and 14 zirconolite grains for this study. For the detailed U–Pb data and trace element data of all samples we refer the interested reader to the Supplementary Data.

4.1. U–Pb Dating of Zircons

For zircon inclusions in gem-quality ruby and spinel showing growth zoning patterns in VPSE imaging (e.g., Figure 3c), we analysed both core and rim separately. Individual spots from zircon core reveal a wide range of ages, from ~94 Ma to ~26 Ma (Figure 4a). The zircon rim displays ages between ~30 Ma to ~22 Ma (Figure 4a). The youngest ages are concordant at 22.26 ± 0.36 Ma for zircon in ruby (Figure 5a) and 22.88 ± 0.72 Ma for zircon in spinel (Figure 5b).

In the ruby- and spinel-bearing Bawlongyi marble, we observed both zircon and zirconolite as accessory mineral phases. The U–Pb ages of zircon grains cover a wide range from Cretaceous (~95 Ma) to Early Miocene (~17 Ma, Figure 4b). This is similar to the zircon inclusions in gemstones. The youngest age of zircon is concordant at 17.11 ± 0.22 Ma (Figure 5c) which is younger than that from our investigated rubies and spinels. The core ages from accessory zircon intergrown with zirconolite reveal ages ranging from ~65 Ma to ~55 Ma. These ages are within the range as the age of zircon cores found in gemstones (ruby and spinel).

Analysed zircon core results in garnet-orthopyroxene gneiss from Aunglan Taung yield groups of Jurassic (~180 Ma to ~140 Ma) and Cretaceous (~110 Ma to ~70 Ma) ages (Figure 6). The U–Pb ages of zircon rims were found to be concordant at 31.98 ± 0.30 Ma, as is shown in Figure 5d.

U–Pb ages of accessory zircon in biotite-garnet gneiss from Kinn reveal mainly discordant ages (Supplementary Figure S2). Two zircon rim measurements give a concordant age of 26.13 ± 1.24 Ma (Figure 5e). These rim ages are also consistent with ages of zircon rims in gemstones from the present study. The discordia may correspond to a mixture with different overgrowth ages, or Pb loss. The oldest zircon core age is ~985 Ma, and a VPSE image of this zircon is shown in Supplementary Figure S3.
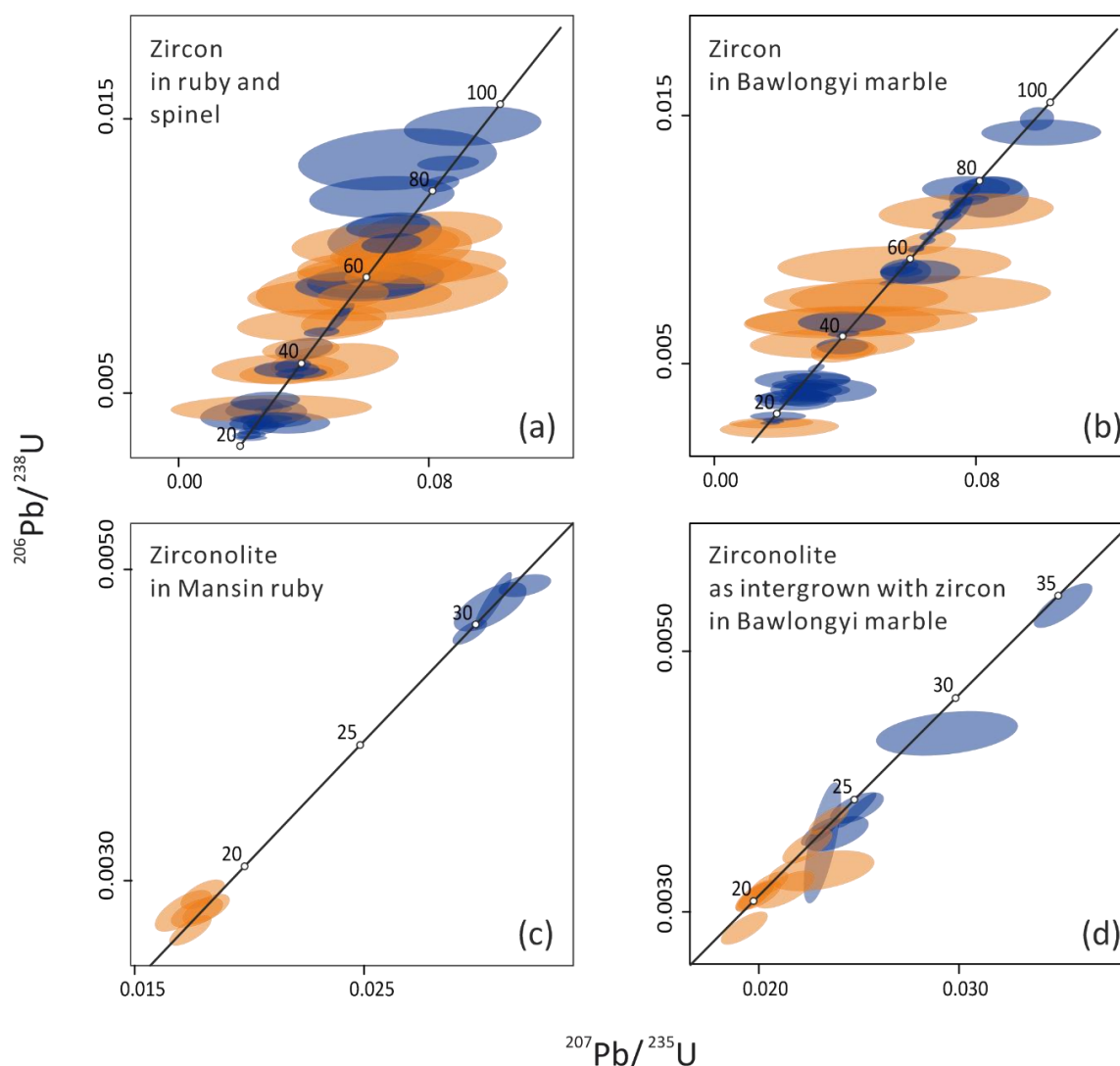
Figure 4. Wetherill diagrams showing wide range of U–Pb age of (**a**) zircon inclusion in gem-quality ruby and spinel, (**b**) accessory zircon in Bawlongyi marble, (**c**) zirconolite inclusion in ruby from Mansin and (**d**) zirconolite intergrown with zircon in Bawlongyi marble. Ellipses indicate two standard error (2SE) uncertainty of measurements. Blue is by sector-field (SF)-MS and orange is by time-of-flight (TOF)-MS.

4.2. U–Pb Dating of Zirconolite

Zirconolite grains from Mansin ruby and from ruby- and spinel-bearing marble (Bawlongyi) were analysed by TOF-MS and SF-MS, as shown in Figure 4c,d. Zirconolite from Mansin ruby reveals a concordia age of 29.78 ± 0.38 Ma (Figure 5f) analysed by SF-MS, whereas TOF-MS analysis adjacent to the SF-MS measurements reveals an age of 18.06 ± 0.36 Ma (Figure 5g). Furthermore, zirconolites observed as intergrowth of zircons in ruby- and spinel-bearing marble yield apparent concordia ages at 23.61 ± 0.36 Ma using the SF-MS setup (Figure 5h) and 20.30 ± 0.30 Ma using the TOF-MS (Figure 5i). These different results for zirconolite may be due to different growth zonings in the inclusions, which could not be identified by VPSE imaging. The discrepancy may also be due to the application of a non-matrix matched standard (zircon), which induces various fractionation effects with different instrument operating parameters and corrections [53,64]. Since both measurements have revealed secondary reference zircon (Zircon91500) in accordance with the published ages within uncertainty, the two instrumental setups were operated normally. Therefore, the reported zirconolite ages may lack of accuracy and 2SE of uncertainty is related to measurement precision. Due to lack of a zirconolite

reference material, it is important to mention that the zirconolite ages obtained here may be only indicative and can be improved further.
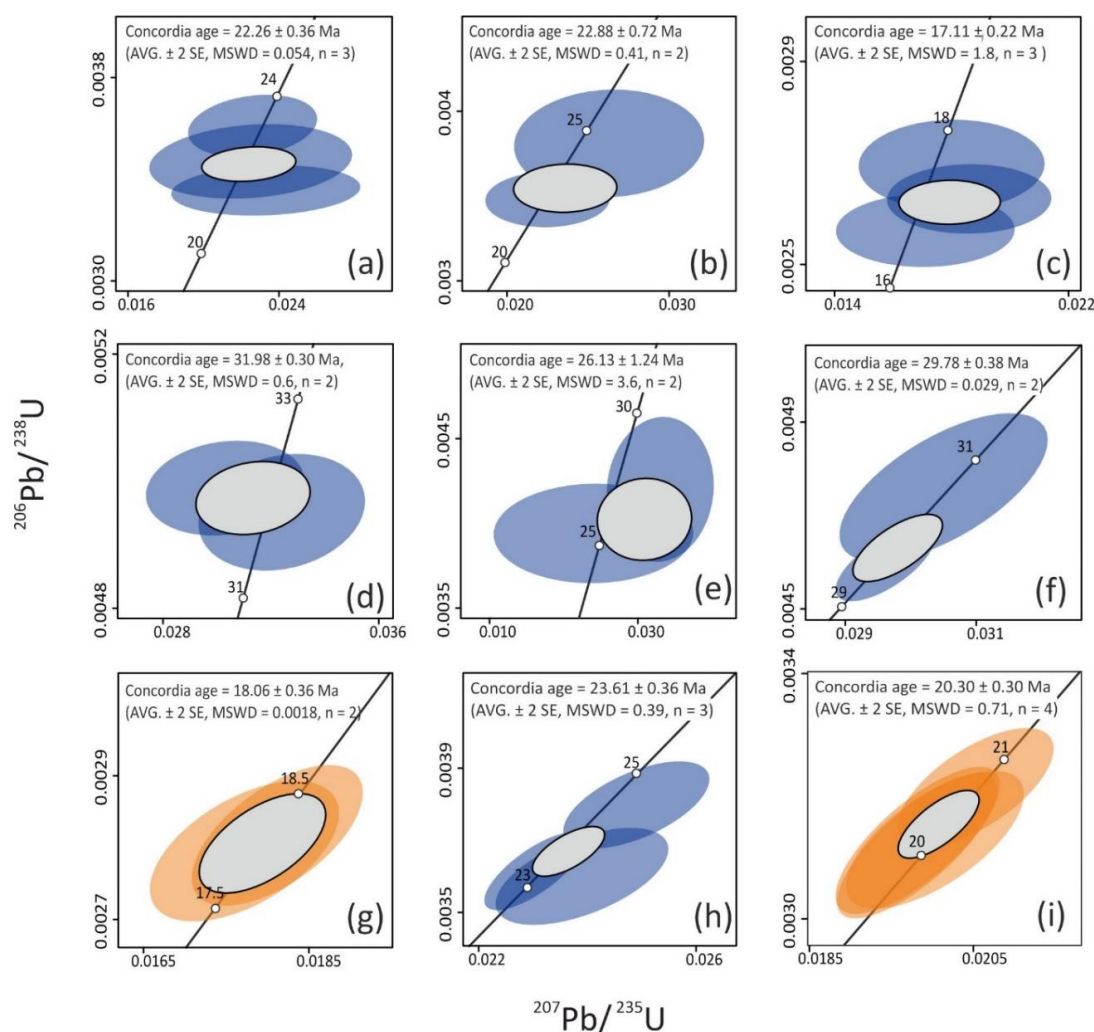

Figure 5. Concordia ages analysed on the rim of zircon inclusion in (**a**) Mansin and Kyatpyin ruby (22.26 ± 0.36 Ma), (**b**) Kyauksin spinel (22.88 ± 0.72 Ma) and accessory zircon in (**c**) Bawlongyi marble (17.11 ± 0.22 Ma), (**d**) Aunglan Taung gneiss (31.98 ± 0.30 Ma) and (**e**) Kinn gneiss (26.13 ± 1.24 Ma). Concordia age of zirconolite inclusion from Mansin ruby showing (**f**) 29.78 ± 0.38 Ma by SF-MS, and (**g**) 18.06 ± 0.36 Ma by TOF-MS as well as of zirconolite intergrown with zircon in Bawlongyi marble showing (**h**) 23.61 ± 0.36 Ma by SF-MS, (**i**) 20.30 ± 0.30 Ma by TOF-MS. Reported ages are concordia ages with two standard error (2SE) of uncertainty of measurements. Blue ellipses are by SF-MS and orange ellipses are by TOF-MS with 2SE of uncertainty. Gray ellipses indicate concordia age with 1SE of uncertainty.

## 4.3. REE Composition of Zircon and Zirconolite

Using TOF-MS, we collected multi-element data, specifically of the rare earth elements (REE), simultaneously to the U–Pb measurements. For a detailed list of the REE concentrations of selected zircon and zirconolite samples present as inclusions in ruby and spinel and as accessory minerals in host rock (Bawlongyi marble) and adjacent gneisses (Aunglan Taung gneiss and Kinn gneiss) the reader is referred to Supplementary Data. Most of the zircon REE data are from the core of the inclusions/accessory minerals, whereas in the zirconolite no zoning was observed by VPSE imaging.

The chondrite-normalized Coryell-Masuda diagrams of our samples reveal for zircon a distinct enrichment in heavy REE (HREE) in all samples [50]. Zircon inclusions from gem-quality ruby

(Figure 7a) vary quite largely in their REE concentrations, thus resulting in a rather broad REE pattern in the chondrite-normalized plot. Still, all investigated zircon inclusions in ruby show a very similar trend with part of light REE (LREE) at or even below detection limit. In addition, they show only a weak negative Eu anomaly and no positive Ce anomaly. The REE pattern of zircon in spinel (blue traces in Figure 7a) follows the same trend, but in addition these inclusions contain even less LREE, mostly below detection limit.
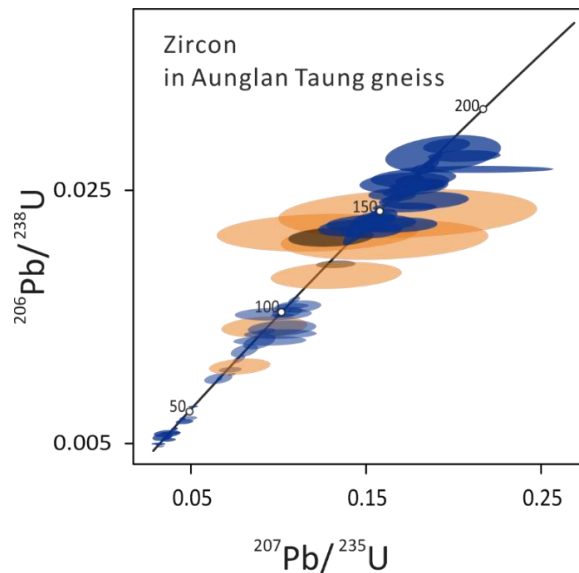
Figure 6. Wetherill diagram of accessory zircon in Aunglan Taung gneiss. Ages of accessory zircon in Kinn gneiss show discordia ages and are reported in Supplementary Figure S2. Ellipses indicate two standard error (2SE) uncertainty of measurements. Blue is by SF-MS and orange is by TOF-MS.
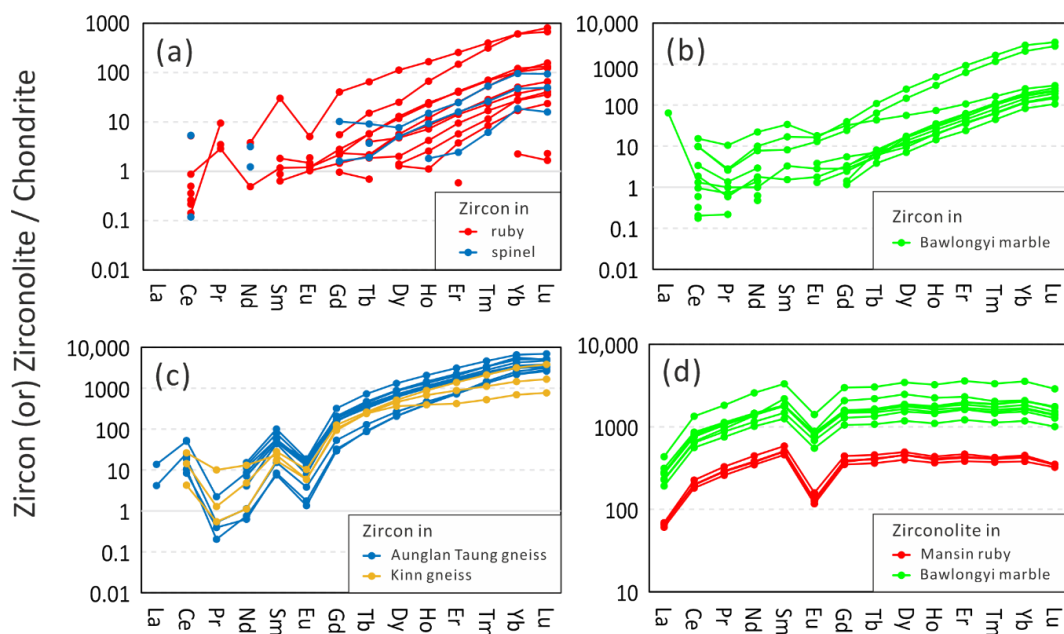
Figure 7. Chondrite normalized Coryell-Masuda rare earth element (REE) diagrams of (**a**) zircon inclusion in gem-quality ruby and spinel (**b**) marble (**c**) gneiss and (**d**) zirconolite from ruby and marble. (Chondrite REE values from [65]).

Zircon as accessory mineral in Bawlongyi marble (Figure 7b) shows a very similar pattern as the zircon inclusions in ruby, again with only a weak negative Eu anomaly, but in contrast to the zircon inclusions in ruby with a (weak) positive Ce anomaly. In general, the concentrations of REE in zircons from the marble are higher than from zircon inclusions in ruby (and spinel), as can also be seen in the chondrite-normalized plot. The most pronounced enrichment in HREE is observed in zircons from the gneiss samples (Aunglan Taung and Kinn) (Figure 7c). In addition, these zircons show also distinct negative Eu and positive Ce anomalies.

Compared to zircon, the analysed zirconolites show a distinctly different REE pattern in their chondrite-normalized plot (Figure 7d). Both, zirconolite as inclusions in ruby (from Mansin) and as accessory minerals in marble host rock (Bawlongyi) reveal a rather flat REE pattern, dominated by a distinct negative Eu anomaly and a general relative depletion in LREE. Similar to the zircon inclusions in ruby (and spinel), the concentration of REE is lower in the zirconolite inclusions in gem-quality ruby than in the host-rock (Bawlongyi marble).

5. Discussion and Conclusions

The zircons from gemstone samples and ruby- and spinel-bearing marble from Mogok area reveal consistent radiometric U–Pb ages over a wide time range from Cretaceous to Early Miocene. The youngest ages (Late Oligocene to Early Miocene) are found in the rim of accessory zircon in the Bawlongyi marble. They are in good agreement with previously reported U–Pb ages on zircon inclusions [16], as well as on a titanite inclusion in ruby from Thurein Taung (western Mogok) [14]. Similar U–Pb ages are also known from analyses carried out by commercial gemmological laboratories on faceted gem-quality ruby and sapphire from Mogok [17–19].

The U–Pb ages calculated in the rim of zircon indicate a late regional metamorphic event and are interpreted to be related to the formation of the marble-hosted ruby and spinel in the Mogok area. The youngest concordia ages recorded from the rim of zircon inclusions in our studied gemstones are 22.26 ± 0.36 Ma (ruby) and 22.88 ± 0.72 Ma (spinel). Based on the evident similarity of ages of the zircon rims in both, ruby and spinel, we presume that ruby and spinel both formed during Oligocene to Early Miocene and under similar granulite-facies regional metamorphic conditions as recorded in the surrounding Mogok area [4,35,66,67]. Interestingly, the youngest age of zircon grains in Bawlongyi marble is even younger with 17.11 ± 0.22 Ma. This is interpreted to be related to post-regional metamorphic contact metamorphism [2,26,45,68] caused by the late intrusion of Kabaing granite nearby (Figure 2). This youngest zircon age is in accordance with dating results on zircons from Kabaing granite (16.8 ± 0.5 Ma) [26]. A comparison of geochronological data from this study with previously reported data from literature is presented in Figure 8.

Moreover, we observe two age groups in the core of accessory zircon in the garnet-orthopyroxene gneiss from Aunglan Taung (central Mogok): (1) Jurassic and (2) Cretaceous (Figure 6). Jurassic zircon ages were previously recorded in granite from the Mogok area [2] and in orthogneiss of Kyanigan Hills close to the Mogok area [39]. According to Mitchell [69] and references therein, the Mogok belt was considered as a former northward continuation of the Sumatra-western Myanmar Late Cretaceous magmatic arc, as suggested by several age results on granodioritic to tonalitic plutons and batholiths from Banmauk area. The youngest rim ages of zircon grains in Aunglan Taung gneiss reveal a concordia age at 31.98 ± 0.30 Ma, similar ages have been reported in other studies [16,70]. Accessory zircon in the biotite-garnet gneiss from Kinn area shows discordant ages. The oldest U–Pb ages (Precambrian) are found in the core of a zircon grain, which we interpreted as a detrital zircon based on its growth zoning pattern (see Supplementary Figure S3).

These old age results are in accordance with former studies which attribute the metasediments of Mogok a Precambrian age [27,28,41]. The Late Oligocene ages (e.g., 26.39 ± 1.24 Ma) from zircon rims in Kinn gneiss are interpreted to represent the most recent regional metamorphic event.
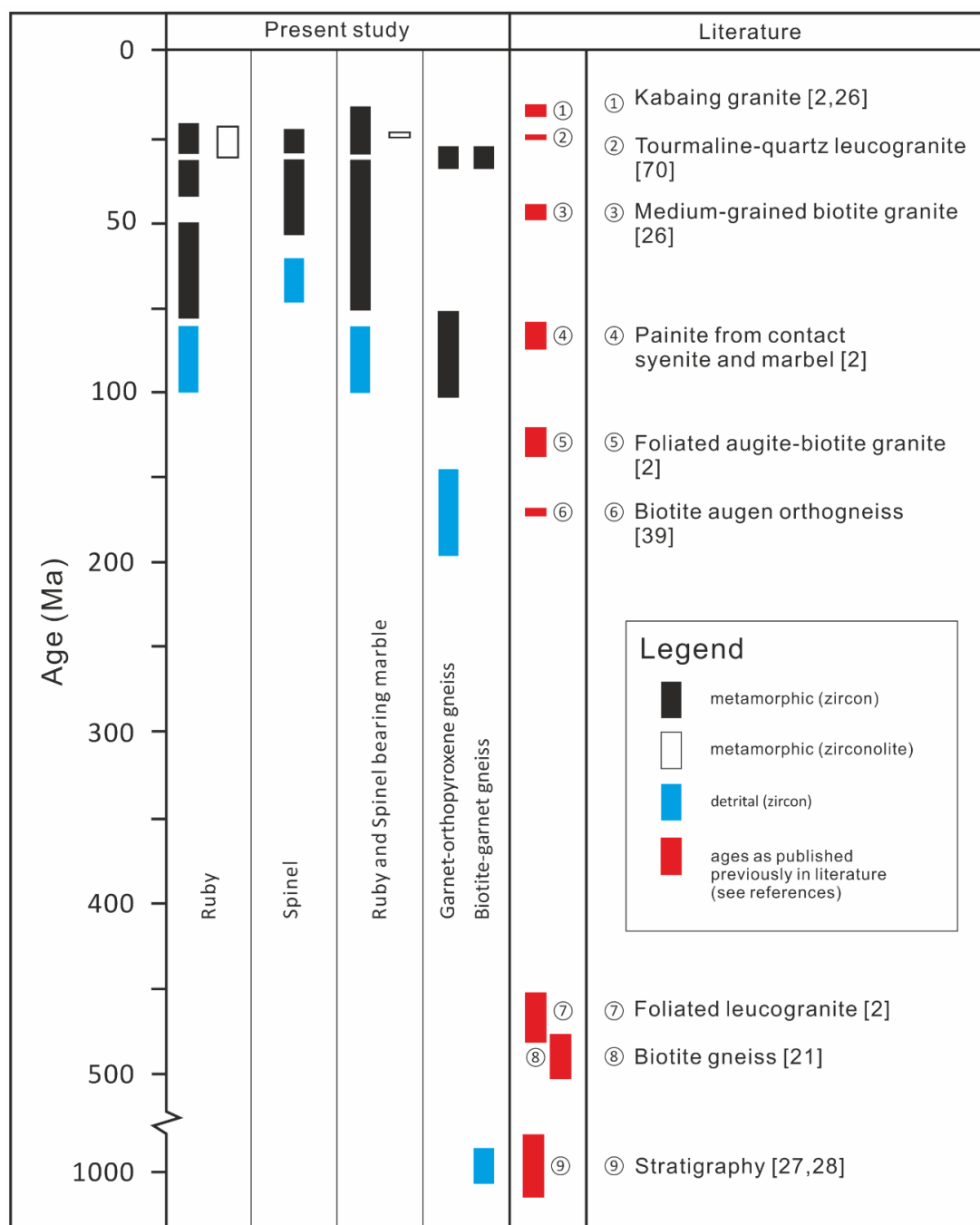
Figure 8. U–Pb ages reported in this study compared to previously published ages from the Mogok Stone Tract.

Zirconolite in ruby from Mansin reveals a U–Pb age of 18.06 ± 0.36 Ma using TOF-MS and 29.78 ± 0.38 Ma using SF-MS. A difference is also observed with zirconolite intergrown with zircon in ruby- and spinel-bearing marble (20.30 ± 0.30 Ma with TOF-MS and 23.61 ± 0.36 Ma with SF-MS). This discrepancy is discussed in previous section. Despite these differences, the U–Pb ages are still within the range of those previously reported in literature [2,20,21,28]. Further research is ongoing to understand the cause of this discrepancy and to find a method to eliminate it in order to obtain more accurate U–Pb ages on zirconolite.

To summarize, our U–Pb ages on zircon and zirconolite found as inclusions in gem-quality ruby and spinel and as accessory minerals in ruby- and spinel-bearing marble and in adjacent granulite-facies gneisses are well in agreement with data from the wider Mogok area reported

previously in literature [14,21,38–40,68,71]. To visualize this larger context, Figure 9 presents a summary of U–Pb ages from this study together with U–Pb data of the wider Mogok area [72]. Based on the results of this study and in accordance with previous investigations, we conclude that the Mogok area and its surroundings experienced a Paleogene granulite-facies regional metamorphic overprint, influenced by post-collisional tectonics of the Eurasian and Indian plates [70,73]. We further assume that the marble-hosted gem-quality ruby and spinel of the Mogok Stone Tract formed during this regional metamorphic event between 30 Ma and 22 Ma, i.e., from Oligocene to Early Miocene.
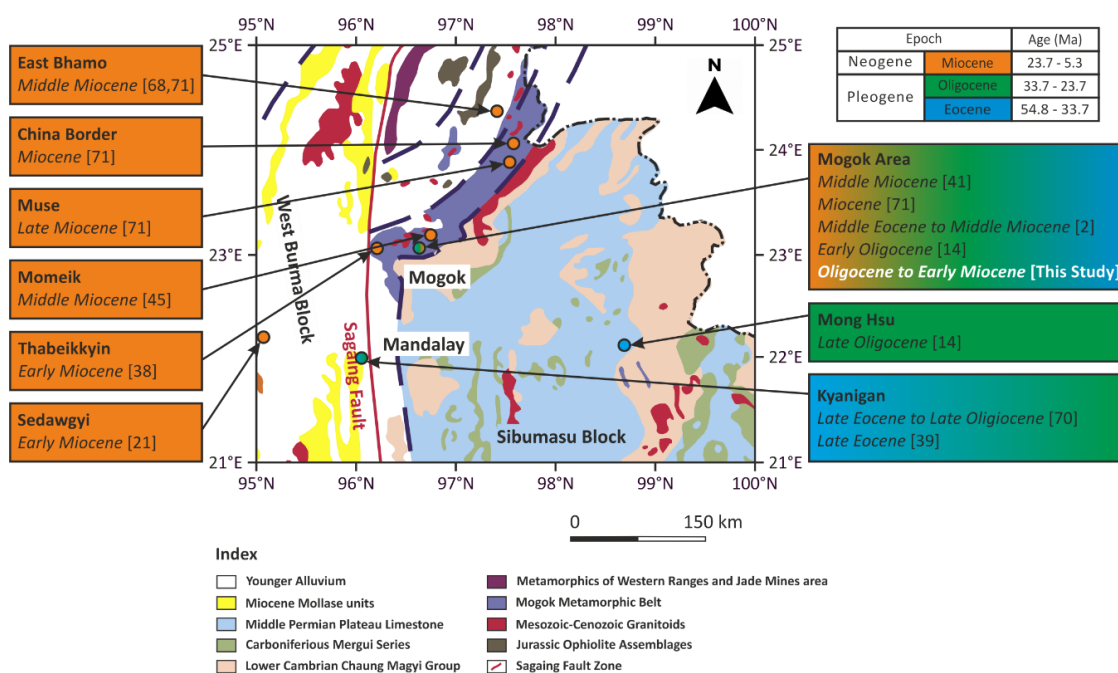
Figure 9. Map showing current research of Mogok combined with previous geochronological studies in its surrounding area (modified after [74] with permission).

Simultaneously to U–Pb dating measurements, REE concentrations in zircon and zirconolite were measured by LA-ICP-TOF-MS and chondrite-normalized REE diagrams were plotted in Figure 7a–d. A positive Ce anomaly and a negative Eu anomaly such as observed in the investigated accessory zircons in Aunglan Taung and Kinn gneisses (Figure 7c) are common in zircon [75,76] and generally related to magmatic fractionation processes (e.g., by feldspar crystallizations and/or a function of the oxygen fugacity and the Eu anomaly of the melt) [77]. Our focus is to characterize the studied zircon and zirconolite inclusions and accessory minerals from Mogok (Myanmar). Specifically, as to our knowledge, it is the first time that the full range of REEs in zirconolite from Mogok is reported. The zircon and zirconolite REE concentrations (see Supplementary Data) and REE plots may aid in country of origin determination for gem-quality ruby and spinels in commercial gemmological laboratories, similar to a study on apatite inclusions in gem-quality corundum and spinel from Mogok and other deposits [78].

The present study adds considerable new geochronological (U–Pb) and geochemical (REE) data to previous research about the Mogok area in Myanmar. With a special focus on zircon and zirconolite present as inclusions in gem-quality ruby and spinel and as accessory minerals in their marble host rock and adjacent gneisses, our data provides a better understanding of ruby and spinel formation within the Mogok Stone Tract, one of the finest ruby and spinel sources in the world.

mineral in Kinn gneiss, where an oldest age was found in this study, Table S1: LA-ICP-MS instrument operating parameters. Supplementary Data: U–Pb age result and REE concentration in zircon and zirconolite.

References

1. Gordon, R. On the Ruby Mines near Mogok, Burma. *Proc. R. Geogr. Soc. Mon. Rec. Geogr.* **1888**, *10*, 261–275. [CrossRef]

2. Thu, K. The Igneous Rocks of the Mogok Stone Tract: Their Distribution, Petrography, Petrochemistry, Sequence, Geochronology and Economic Geology. Ph.D. Thesis, University of Yangon, Yangon, Myanmar, 2007.

3. Themelis, T. *Gems and Mines of Mogok*; A&T Pub.: Los Angeles, CA, USA, 2008.

4. Phyo, M.M. Mineralogical, Gemmological and Petrological Study of the Mogok Stone Tract in Myanmar with a Special Focus on Gem-Quality Ruby and Spinel. Ph.D. Thesis, Universität Basel, Basel, Switzerland, 2019.

5. Harlow, G.E.; Bender, W. A study of ruby (corundum) compositions from the Mogok Belt, Myanmar: Searching for chemical fingerprints. *Am. Mineral.* **2013**, *98*, 1120–1132. [CrossRef]

6. Sutherland, F.L.; Zaw, K.; Meffre, S.; Yui, T.-F.F.; Thu, K. Advances in trace element "fingerprinting" of gem corundum, ruby and sapphire, Mogok area, Myanmar. *Minerals* **2014**, *5*, 61–79. [CrossRef]

7. Giuliani, G.; Fallick, A.E.; Garnier, V.; France-Lanord, C.; Ohnenstetter, D.; Schwarz, D. Oxygen isotope composition as a tracer for the origins of rubies and sapphires. *Geology* **2005**, *33*, 249–252. [CrossRef]

8. Yui, T.F.; Zaw, K.; Wu, C.M. A preliminary stable isotope study on Mogok Ruby, Myanmar. *Ore Geol. Rev.* **2008**, *34*, 192–199. [CrossRef]

9. Zaw, K.; Sutherland, L.; Yui, T.-F.; Meffre, S.; Thu, K. Vanadium-rich ruby and sapphire within Mogok Gemfield, Myanmar: Implications for gem color and genesis. *Miner. Depos.* **2015**, *50*, 25–39. [CrossRef]

10. Giuliani, G.; Fallick, A.E.; Boyce, A.J.; Pardieu, V.; Pham, V.L. Pink and red spinels in marble: Trace elements, oxygen isotopes, and sources. *Can. Mineral.* **2017**, *55*, 743–761. [CrossRef]

11. Phyo, M.M.; Franz, L.; Bieler, E.; Balmer, W.; Krzemnicki, M.S. Spinel from Mogok, Myanmar–A detailed inclusion study by raman microspectroscopy and scanning electron microscopy. *J. Gemmol.* **2019**, *36*, 418–435. [CrossRef]

12. Giuliani, G.; Dubessy, J.; Banks, D.A.; Lhomme, T.; Ohnenstetter, D. Fluid inclusions in ruby from Asian marble deposits: Genetic implications. *Eur. J. Mineral.* **2015**, *27*, 393–404. [CrossRef]

13. Sutherland, F.L.; Piilonen, P.C.; Zaw, K.; Meffre, S.; Thompson, J. Sapphire within zircon-rich gem deposits, Bo Loei, Ratanakiri Province, Cambodia: Trace elements, inclusions, U–Pb dating and genesis. *Aust. J. Earth Sci.* **2015**, *62*, 761–773.

14. Sutherland, F.; Zaw, K.; Meffre, S.; Thompson, J.; Goemann, K.; Thu, K.; Nu, T.; Zin, M.; Harris, S. Diversity in ruby geochemistry and its inclusions: Intra- and inter-continental comparisons from Myanmar and Eastern Australia. *Minerals* **2019**, *9*, 28. [CrossRef]

15. Coenraads, R.R.; Lin Sutherland, F.; Kinny, P.D. The origin of sapphires: U–Pb dating of zircon inclusions sheds new light. *Mineral. Mag.* **1990**, *54*, 113–122. [CrossRef]

16. Zaw, K.; Sutherland, F.L.; Graham, I.; Meffre, S.; Thu, K. Dating zircon inclusions in gem corundum deposits and genetic implications. In Proceedings of the 13th Quardrennial IAGOD Symposium, Adelaide, Australia, 6–9 April 2010.

17. Elmaleh, E.; Schmidt, S.T.; Karampelas, S.; Link, K.; Kiefert, L.; Süssenberger, A.; Paul, A. U–Pb ages of zircon inclusions in sapphires from Ratnapura and Balangoda (Sri Lanka) and implications for geographic origin. *GEMS Gemol.* **2019**, *55*, 18–28.

18. Krzemnicki, M.S.; Wang, H.A.O.; Phyo, M.M. Age dating applied as a testing procedure to gemstones and biogenic gem materials. In Proceedings of the 36th IGC Conference, Nante, France, 27–31 August 2019; pp. 48–50.

19. Link, K. Age Determination of zircon inclusions in faceted sapphires. *J. Gemmol.* **2016**, *34*, 692–700. [CrossRef]

20. Garnier, V.; Maluski, H.; Giuliani, G.; Ohnenstetter, D.; Schwarz, D. Ar–Ar and U–Pb ages of marble-hosted ruby deposits from central and southeast Asia. *Can. J. Earth Sci.* **2006**, *43*, 509–532. [CrossRef]

21. Mitchell, A.; Chung, S.L.; Oo, T.; Lin, T.H.; Hung, C.H. Zircon U–Pb ages in Myanmar: Magmatic-metamorphic events and the closure of a neo-Tethys ocean? *J. Asian Earth Sci.* **2012**, *56*, 1–23. [CrossRef]

22. Sutherland, F.L.; Duroc-Danner, J.M.; Meffre, S. Age and origin of gem corundum and zircon megacrysts from the Mercaderes-Rio Mayo area, South-west Colombia, South America. *Ore Geol. Rev.* **2008**, *34*, 155–168. [CrossRef]

23. Sorokina, E.S.; Rösel, D.; Häger, T.; Mertz-Kraus, R.; Saul, J.M. LA-ICP-MS U–Pb dating of rutile inclusions within corundum (ruby and sapphire): New constraints on the formation of corundum deposits along the Mozambique belt. *Miner. Depos.* **2017**, *52*, 641–649. [CrossRef]

24. Link, K. New age data for blue sapphire from Mogok, Myanmar. *J. Gemmol.* **2016**, *35*, 107–109.

25. Balmer, W.A.; Hauzenberger, C.A.; Fritz, H.; Sutthirat, C. Marble-hosted ruby deposits of the Morogoro Region, Tanzania. *J. Afr. Earth Sci.* **2017**, *134*, 626–643. [CrossRef]

26. Gardiner, N.J.; Robb, L.J.; Morley, C.K.; Searle, M.P.; Cawood, P.A.; Whitehouse, M.J.; Kirkland, C.L.; Roberts, N.M.W.; Myint, T.A. The tectonic and metallogenic framework of Myanmar: A Tethyan mineral system. *Ore Geol. Rev.* **2016**, *79*, 26–45. [CrossRef]

27. Chhibber, H.L. *The Geology of Burma*; Macmillan and Co. Limited: London, UK, 1934.

28. Iyer, L.A.N. *The Geology and Gem-Stones of the Mogok Stone Tract, Burma. Memoirs of the Geological Survey of India*; Calcutta: Delhi, India, 1953; Volume 82.

29. Mitchell, A.H.G.; Htay, M.T.; Htun, K.M.; Win, M.N.; Oo, T.; Hlaing, T. Rock relationships in the Mogok metamorphic belt, Tatkon to Mandalay, central Myanmar. *J. Asian Earth Sci.* **2007**, *29*, 891–910. [CrossRef]

30. Bertrand, G.; Rangin, C.; Maluski, H.; Han, T.A.; Thein, M.; Myint, O.; Maw, W.; Lwin, S. Cenozoic metamorphism along the Shan scarp (Myanmar): Evidences for ductile shear along the Sagaing fault or the northward migration of the eastern Himalayan syntaxis? *Geophys. Res. Lett.* **1999**, *26*, 915–918. [CrossRef]

31. Bender, F. *Geology of Burma*; Schweizerbart Science Publishers: Stuttgart, Germany, 1983.

32. Zaw, K. Geological, petrological and geochemical characteristics of granitoid rocks in Burma: With special reference to the associated W-Sn mineralization and their tectonic setting. *J. Southeast Asian Earth Sci.* **1990**, *4*, 293–335. [CrossRef]

33. Gardiner, N.J.; Searle, M.P.; Morley, C.K.; Whitehouse, M.P.; Spencer, C.J.; Robb, L.J. The closure of Palaeo-Tethys in Eastern Myanmar and Northern Thailand: New insights from zircon U–Pb and Hf isotope data. *Gondwana Res.* **2016**, *39*, 401–422. [CrossRef]

34. Lee, H.Y.; Chung, S.L.; Yang, H.M. Late Cenozoic volcanism in central Myanmar: Geochemical characteristics and geodynamic significance. *Lithos* **2016**, *245*, 174–190. [CrossRef]

35. Thu, Y.K.; Win, M.M.; Enami, M.; Tsuboi, M. Ti–rich biotite in spinel and quartz–bearing paragneiss and related rocks from the Mogok metamorphic belt, central Myanmar. *J. Mineral. Petrol. Sci.* **2016**, *111*, 270–282.

36. La Touche, T.H.D. *Geology of the Northern Shan State*; Office of the Geological Survey of India: Calcutta, India, 1913.

37. Thein, M. Modes of occurrence and origin of precious gemstone deposits of the Mogok Stone Tract. *J. Myanmar Geosci. Soc.* **2008**, *1*, 75–84.

38. Brook, M.; Snelling, N.J. K/Ar and Rb/Sr age determinations on rocks and minerals from Burma. In *Report of the Isotope Geology Unit 76/12*; Institute of Geological Science: Keyworth, Nottingham, UK, 1976.

39. Barley, M.E.; Pickard, A.L.; Zaw, K.; Rak, P.; Doyle, M.G. Jurassic to Miocene magmatism and metamorphism in the Mogok metamorphic belt and the India-Eurasia collision in Myanmar. *Tectonics* **2003**, *22*, 1–11. [CrossRef]

40. Searle, M.P.; Waters, D.J.; Morley, C.K.; Gardiner, N.J.; Htun, U.K.; Nu, T.T.; Robb, L.J. Chapter 12 Tectonic evolution of the Mogok metamorphic and Jade mines belts and ophiolitic terranes of Burma (Myanmar). In *Myanmar: Geology, Resources and Tectonics*; Barber, A.J., Zaw, K., Crow, M.J., Eds.; Geological Society: London, UK, 2017; Volume 48, pp. 261–293.

41. Searle, D.L.; Haq, B.T. The Mogok belt of Burma and its relationship to the Himalayan orogeny. In Proceedings of the 22nd International Geological Congress, New Delhi, India, 14–22 December 1964; Volume 22, pp. 132–161.

42. Clegg, E.L.G. The Cretaceous and associated rocks of Burma. *Mem. Geol. Surv. India* **1941**, *74*, 1–102.

43. Sone, M.; Metcalfe, I. Parallel Tethian sutures in mainland Sout-East Asia: New insights for Palaeo-Tethys closure and implications for the Indosinian Orogeny. *C. R. Geosci.* **2008**, *340*, 166–179. [CrossRef]

44. Zaw, K.; Swe, K.; Barber, A.J.; Crow, M.J.; Nwe, Y.Y. Chapter 1 Introduction to the geology of Myanmar. In *Myanmar: Geology, Resources and Tectonics*; Barber, A.J., Zaw, K., Crow, M.J., Eds.; Geological Society: London, UK, 2017; Volume 48.

45. Damon, P.E. *Granities from the Kabaing Batholithic Complex, Mogok Area, Burma*; Correlation and Chronology of ore Deposits and Volcanic Rocks; Annual Progress Report No. C00-689-60; United States Atomic Energy Commission: Washington, DC, USA, 1966.

46. Phyo, M.M.; Franz, L.; De Capatini, C.; Balmer, A.W.; Krzemnicki, M.S. Petrology and PT-conditions of quartz- and nepheline-bearing gneisses from Mogok Stone Tract, Myanmar. In Proceedings of the 15th Swiss Geoscience Meeting, Davos, Switzerland, 17–18 November 2017.

47. Bayliss, P.; Mazzi, F.; Munno, R.; White, T.J. Mineral nomenclature: Zirconolite. *Mineral. Mag.* **1989**, *53*, 565–569. [CrossRef]

48. Hughes, R.W. *Ruby & Sapphire*; RWH Publishing: Bangkok, Thailand, 1997.

49. Schaltegger, U.; Schmitt, A.K.; Horstwood, M.S.A. U–Th–Pb zircon geochronology by ID-TIMS, SIMS, and laser ablation ICP-MS: Recipes, interpretations, and opportunities. *Chem. Geol.* **2015**, *402*, 89–110. [CrossRef]

50. Hoskin, P.W.O.; Schaltegger, U. The Composition of Zircon and Igneous and Metamorphic Petrogenesis. *Rev. Mineral. Geochem.* **2003**, *53*, 27–62. [CrossRef]

51. Hendriks, L.; Gundlach-Graham, A.; Hattendorf, B.; Günther, D. Characterization of a new ICP-TOFMS instrument with continuous and discrete introduction of solutions. *J. Anal. At. Spectrom.* **2017**, *32*, 548–561. [CrossRef]

52. Wang, H.A.O.; Krzemncki, M.S. Multi-Element Analysis of Minerals using Laser Ablation Inductively Coupled Plasma Time Of Flight Mass Spectrometry. Manuscript near submission.

53. Jackson, S.E.; Pearson, N.J.; Griffin, W.L.; Belousova, E.A. The application of laser ablation-inductively coupled plasma-mass spectrometry to in situ U–Pb zircon geochronology. *Chem. Geol.* **2004**, *211*, 47–69. [CrossRef]

54. Horstwood, M.S.A.; Košler, J.; Gehrels, G.; Jackson, S.E.; McLean, N.M.; Paton, C.; Pearson, N.J.; Sircombe, K.; Sylvester, P.; Vermeesch, P.; et al. Community-Derived Standards for LA-ICP-MS U–(Th–)Pb Geochronology–Uncertainty Propagation, Age Interpretation and Data Reporting. *Geostand. Geoanal. Res.* **2016**, *40*, 311–332. [CrossRef]

55. Sláma, J.; Košler, J.; Condon, D.J.; Crowley, J.L.; Gerdes, A.; Hanchar, J.M.; Horstwood, M.S.A.; Morris, G.A.; Nasdala, L.; Norberg, N.; et al. Plešovice zircon—A new natural reference material for U–Pb and Hf isotopic microanalysis. *Chem. Geol.* **2008**, *249*, 1–35. [CrossRef]

56. Black, L.P.; Kamo, S.L.; Allen, C.M.; Aleinikoff, J.N.; Davis, D.W.; Korsch, R.J.; Foudoulis, C. TEMORA 1: A new zircon standard for phanerozoic U–Pb geochronology. *Chem. Geol.* **2003**, *200*, 155–170. [CrossRef]

57. Wiedenbeck, M.; Alle, P.; Corfu, F.; Griffin, W.L.; Meier, M.F.O.; von Quadt, A.; Roddick, J.C.; Spiegel, W. Three natural zircon standards for U–Th–Pb, Lu–Hf, trace element and REE analyses. *Geostand. Newsl.* **1995**, *19*, 1–23. [CrossRef]

58. Paton, C.; Hellstrom, J.; Paul, B.; Woodhead, J.; Hergt, J. Iolite: Freeware for the visualisation and processing of mass spectrometric data. *J. Anal. At. Spectrom.* **2011**, *26*, 2508–2518. [CrossRef]

59. Petrus, J.A.; Kamber, B.S. VizualAge: A Novel Approach to Laser Ablation ICP-MS U–Pb Geochronology Data Reduction. *Geostand. Geoanal. Res.* **2012**, *36*, 247–270. [CrossRef]

60. Ulianov, A.; Müntener, O.; Schaltegger, U.; Bussy, F. The data treatment dependent variability of U–Pb zircon ages obtained using mono-collector, sector field, laser ablation ICPMS. *J. Anal. At. Spectrom.* **2012**, *27*, 663–676. [CrossRef]

61. Vermeesch, P. IsoplotR: A free and open toolbox for geochronology. *Geosci. Front.* **2018**, *9*, 1479–1493. [CrossRef]

62. Spencer, C.J.; Kirkland, C.L.; Taylor, R.J.M. Strategies towards statistically robust interpretations of in situ U–Pb zircon geochronology. *Geosci. Front.* **2016**, *7*, 581–589. [CrossRef]

63. Guillong, M.; Hametner, K.; Reusser, E.; Wilson, S.A.; Günther, D. Preliminary Characterisation of New Glass Reference Materials (GSA-1G, GSC-1G, GSD-1G and GSE-1G) by Laser Ablation-Inductively Coupled Plasma-Mass Spectrometry Using 193 nm, 213 nm and 266 nm Wavelengths. *Geostand. Geoanal. Res.* **2005**, *29*, 315–331. [CrossRef]

64. Sylvester, P.J.; Ghaderi, M. Trace element analysis of scheelite by excimer laser ablation-inductively coupled plasma-mass spectrometry (ELA-ICP-MS) using a synthetic silicate glass standard. *Chem. Geol.* **1997**, *141*, 49–65. [CrossRef]

65. McDonougha, W.F.; Sun, S.-S. The composition of the Earth. *Chem. Geol.* **1995**, *120*, 223–253. [CrossRef]

66. Thu, Y.K.; Enami, M.; Kato, T.; Tsuboi, M. Granulite facies paragneisses from the middle segment of the Mogok metamorphic belt, central Myanmar. *J. Mineral. Petrol. Sci.* **2017**, *112*, 1–19.

67. Win, M.M.; Enami, M.; Kato, T. Metamorphic conditions and CHIME monazite ages of Late Eocene to Late Oligocene high-temperature Mogok metamorphic rocks in central Myanmar. *J. Asian Earth Sci.* **2016**, *117*, 304–316. [CrossRef]

68. Bertrand, G.; Rangin, C.; Maluski, H.; Bellon, H. Diachronous cooling along the Mogok Metamorphic Belt (Shan scarp, Myanmar): The trace of the northward migration of the Indian syntaxis. *J. Asian Earth Sci.* **2001**, *19*, 649–659. [CrossRef]

69. Mitchell, A.H.G. Cretaceous-Cenozoic tectonic events in the western Myanmar (Burma)-Assam region. *J. Geol. Soc. Lond.* **1993**, *150*, 1089–1102. [CrossRef]

70. Searle, M.P.; Noble, S.R.; Cottle, J.M.; Waters, D.J.; Mitchell, A.H.G.; Hlaing, T.; Horstwood, M.S.A. Tectonic evolution of the Mogok metamorphic belt, Burma (Myanmar) constrained by U–Th–Pb dating of metamorphic and magmatic rocks. *Tectonics* **2007**, *26*. [CrossRef]

71. Min, M. Thermochronology Applied to Strike-Slip Zones Central America and Myanmar. Ph.D. Thesis, Technische Universität Bergakademie Freiberg, Freiberg, Germany, 2007.

72. Crow, M.J.; Zaw, K. Appendix Geochronology in Myanmar (1964–2017). In *Myanmar: Geology, Resources and Tectonics*; Barber, A.J., Zaw, K., Crow, M.J., Eds.; Geological Society: London, UK, 2017; Volume 48, pp. 713–759.

73. Dewey, J.F.; Cande, S.; Pitman, W.C. Tectonic evolution of the India-Eurasia collision zone. *Eclogae Geol. Helv.* **1989**, *82*, 717–734.

74. Jiang, H.; Li, W.Q.; Jiang, S.Y.; Wang, H.; Wei, X.P. Geochronological, geochemical and Sr–Nd–Hf isotopic constraints on the petrogenesis of Late Cretaceous A-type granites from the Sibumasu Block, Southern Myanmar, SE Asia. *Lithos* **2017**, *268–271*, 32–47. [CrossRef]

75. Hoskin, P.W.O.; Ireland, T.R. Rare earth element chemistry of zircon and its use as a provenance indicator. *Geology* **2000**, *28*, 627–630. [CrossRef]

76. Gieré, R. Zirconolite, allanite and hoegbomite in a marble skarn from the Bergell contact aureole: Implications for mobility of Ti, Zr and REE. *Contrib. Mineral. Petrol.* **1986**, *93*, 459–470. [CrossRef]

77. Trail, D.; Bruce Watson, E.; Tailby, N.D. Ce and Eu anomalies in zircon as proxies for the oxidation state of magmas. *Geochim. Cosmochim. Acta* **2012**, *97*, 70–87. [CrossRef]

78. Bieri, W.; Grobety, B.; Peretti, A.; Hametner, K.; Günther, D. Chemical composition of apatite inclusions in corundum and spinel determined by LA-ICP-MS and its potential for authentication and provenance determination. In Proceedings of the Goldschmidt 2010: Earth, Energy, and the Environment, Knoxville, TN, USA, 13–18 June 2010; p. 89.